

Effects of Stochastic Webs on Chaotic Electron Transport in Semiconductor Superlattices

T. M. Fromhold, A. A. Krokhin,* C. R. Tench, S. Bujkiewicz,† P. B. Wilkinson, F. W. Sheard, and L. Eaves

School of Physics and Astronomy, University of Nottingham, Nottingham NG7 2RD, United Kingdom

(Received 14 September 2000; published 10 July 2001)

We investigate chaotic electron transport in the lowest miniband of a semiconductor superlattice with a tilted magnetic field. This experimentally accessible non-Kolmogorov-Arnol'd-Moser system involves only stationary electric and magnetic fields, but is dynamically equivalent to a time-dependent kicked harmonic oscillator. The onset of chaos strongly delocalizes the electron orbits, thus raising the electrical conductivity. When the cyclotron and Bloch frequencies are commensurate, the phase space is threaded by a stochastic web, which produces a further resonant increase in the conductivity.

DOI: 10.1103/PhysRevLett.87.046803

PACS numbers: 73.21.-b, 05.45.Mt, 05.60.Cd, 73.61.-r

Until 1992, most experimental studies of quantum systems with chaotic classical dynamics were performed on highly excited hydrogenic atoms [1]. Since then, advances in semiconductor nanostructure fabrication and in the laser cooling of atoms [2] have widened the scope of experimental quantum chaology. In semiconductor physics, chaotic electron transport has been explored in quantum dots and antidot arrays [1,3–6], resonant tunneling diodes [7], and doped [8] or driven [9] superlattices (SLs). Despite the diversity of these experiments, they all involve systems in which the transition to chaos occurs by the gradual destruction of stable islands in accordance with the Kolmogorov-Arnol'd-Moser (KAM) theorem [1]. There is also a different class of chaotic dynamics for which the KAM theorem is inapplicable. These “non-KAM” systems are of great interest due to applications in plasma physics and tokamak fusion [10,11], turbulent fluid dynamics [10], ion traps [12], and quasicrystals [10]. But their quantum properties are not well understood [13] and have never been investigated experimentally.

In this Letter, we show that electrons in a GaAs/(Al_{0.3}-Ga_{0.7})As SL with a magnetic field \mathbf{B} applied at an angle θ to the SL axis provide an experimentally accessible non-KAM system. The Hamiltonian originates from an intrinsically *quantum-mechanical* property of the SL: dispersion of the electronic minibands (MBs). For electrons confined to a single MB, the motion reduces to a one-dimensional (1D) simple harmonic oscillator (SHO) driven by a plane wave. Increasing θ from 0° raises the driving force, thereby inducing chaotic dynamics which delocalize the electron orbits. This increases the drift velocity and conductivity. When the Bloch and cyclotron frequencies are commensurate, the electrons undergo diffusive motion through a stochastic web (SW) in phase space [10]. This produces additional resonant increases in the drift velocity, which should be detectable in experiment.

Figure 1 shows the electronic potential energy and lowest MB for a three-terminal SL structure [14]. The SL layers contain wells (barriers) of width $w = 9.3$ nm ($b = 1.3$ nm). Three-terminal SLs are ideal for studying energy band transport because the electrons can be injected directly into a single MB with a small range of energies

proportional to the emitter-base voltage V_b , which can be controlled independently of the voltage V across the undoped SL layers.

Within the tight-binding approximation, the energy-wave-vector dispersion relation for the first MB is $E(\mathbf{k}) = \Delta(1 - \cos k_x d)/2 + \hbar^2(k_y^2 + k_z^2)/2m$, where $\Delta = 26.2$ meV is the MB width, $d = w + b$, and $m = 0.067m_e$ is the effective mass for motion in the y - z plane parallel to the layers. We investigated electron motion, in an electric field $F \propto V$ antiparallel to the SL (x) axis and a tilted magnetic field $\mathbf{B} = (B \cos\theta, 0, B \sin\theta)$, with F and B small enough to neglect inter-MB tunneling. The effective classical Hamiltonian is obtained from $E(\mathbf{k})$ by adding the electrostatic potential energy and making the substitution $\mathbf{p} = \hbar\mathbf{k} \rightarrow \mathbf{p} + e\mathbf{A} = \mathbf{q}$, where e is the magnitude of the electronic charge and the vector potential $\mathbf{A} = (0, xB \sin\theta - zB \cos\theta, 0)$. In this gauge p_y is conserved and the problem reduces to two-dimensional (2D) (x, z) motion described by the Hamiltonian

$$H(x, z, p_x, p_z) = E_T = \frac{\Delta}{2} \left(1 - \cos \frac{p_x d}{\hbar} \right) + \frac{p_z^2}{2m} + \frac{m\omega_c^2}{2} \times [x \sin\theta - (z - z_0) \cos\theta]^2 - eFx, \quad (1)$$

where $\omega_c = Be/m$ and $z_0 = p_y/eB \cos\theta$. The form of the classical orbits is independent of z_0 and E_T , which we

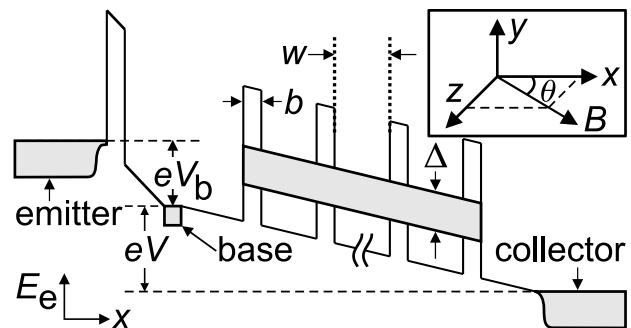


FIG. 1. Schematic conduction band diagram showing electron energy E_e versus x in a three-terminal SL under bias. Shaded regions: energy ranges of lowest SL MB and electrons in n^+ emitter, base, and collector contacts. Inset: orientation of \mathbf{B} .

set to zero. Hamilton's equations show that p_z satisfies an equation of motion

$$\frac{d^2 p_z}{dt^2} + (\omega_c \cos\theta)^2 p_z = - \frac{m\omega_c^2 \Delta d \sin 2\theta}{4\hbar} \times \sin(Kp_z - \omega_B t - \phi), \quad (2)$$

corresponding to a 1D SHO driven by a time- (t -) dependent plane wave of wave number $K = d \tan\theta/\hbar$, angular frequency equal to the Bloch frequency $\omega_B = eFd/\hbar$, and phase $\phi = d[p_x(t=0) + p_z(t=0) \tan\theta]/\hbar$. This non-KAM kicked harmonic oscillator (KHO) has attracted wide theoretical study [10–13,15], but has never been realized in a quantum system.

Classical electron motion in the SL depends *only* on Eq. (2) because the solution, $p_z(t)$, determines $x(t)$, $z(t)$, and $p_x(t)$ for all $\theta \neq 0^\circ$. Figure 2 shows Poincaré sections (PSs) generated for a range of θ by plotting p_z and $q_y = md_y/dt = (\omega_c \cos\theta)^{-1} dp_z/dt = -eB(z \cos\theta - x \sin\theta)$ either when $p_x = 0$ [Figs. 2(a)–2(d)] or at discrete times spaced by the SHO period $T_0 = 2\pi/\omega_c \cos\theta$ [Figs. 2(e) and 2(f)]. We use these two types of PS in order to display the phase space most clearly. In each PS, the distance of each point from the origin equals the lateral momentum $p_L = (q_y^2 + p_z^2)^{1/2}$, which determines the total energy $p_L^2/2m$ of the KHO. In Figs. 2(a)–2(d), this distance also gives the electron position $x = p_L^2/2meF$.

When $\theta = 0^\circ$, the plane wave in Eq. (2) is absent and the motion separates into cyclotron oscillations along z and Bloch oscillations along x [Fig. 3(a)]. Because p_L is conserved, points in the PS [Fig. 2(a)] lie on concentric circles. When $B = 2$ T, the SHO is only weakly perturbed by the plane wave for $\theta \leq 35^\circ$. The phase space for $\theta = 30^\circ$ [Fig. 2(b)] is therefore regular, and the corresponding

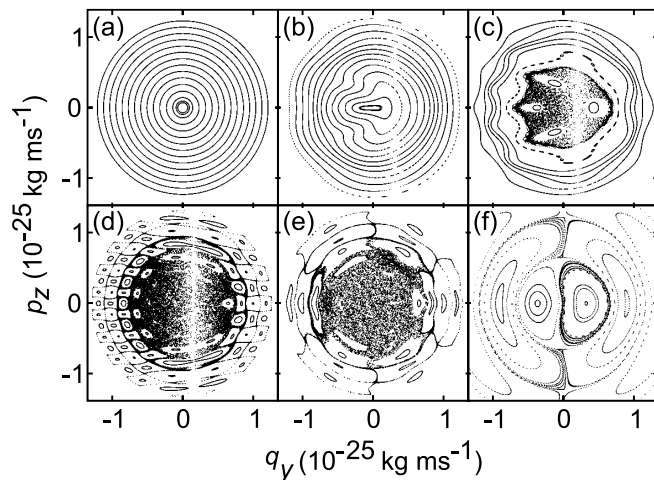


FIG. 2. PSs for $B = 2$ T and (a) $\theta = 0^\circ$, $F = 4.8 \times 10^5$ V m $^{-1}$; (b) $\theta = 30^\circ$, $F = 4.9 \times 10^5$ V m $^{-1}$; (c) $\theta = 45^\circ$, $F = 4.9 \times 10^5$ V m $^{-1}$; (d),(e) $\theta = 60^\circ$, $F = 4.9 \times 10^5$ V m $^{-1}$; (f) $\theta = 30^\circ$, $F = 2.82 \times 10^5$ V m $^{-1}$. Initial conditions in (d)–(f) are chosen so that $\phi = 0$. Vertical gaps in (b)–(d) are a consequence of energy conservation.

electron orbits [Fig. 3(b)] are qualitatively similar to those for $\theta = 0^\circ$.

When $\theta = 45^\circ$, the plane wave in Eq. (2) has maximal amplitude. But it still only weakly perturbs high-energy KHO orbits with $p_L \geq 7 \times 10^{-26}$ kg ms $^{-1}$. These orbits are therefore stable and generate invariant curves in the PS [Fig. 2(c)]. Lower energy orbits are strongly perturbed by the plane wave and produce the chaotic sea in Fig. 2(c). These orbits [Fig. 3(c)] extend much farther along the SL axis than the Bloch oscillations at $\theta = 0^\circ$, because the tilted magnetic field transfers momentum between the x and z directions. This corresponds to the transfer of energy between the KHO and the plane wave in Eq. (2). The six outermost stable loops in Fig. 2(c) enclose the chaotic sea (and four stable islands), thereby limiting the x amplitude of the unstable orbits. But when θ is increased

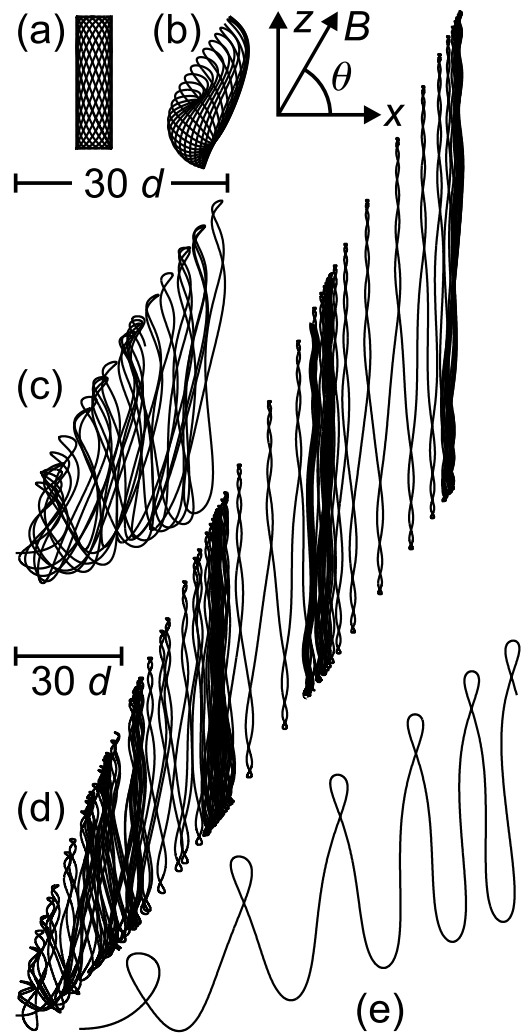


FIG. 3. Electron orbits in the x - z plane for $B = 2$ T and (a) $\theta = 0^\circ$, $F = 4.8 \times 10^5$ V m $^{-1}$; (b) $\theta = 30^\circ$, $F = 4.9 \times 10^5$ V m $^{-1}$; (c) $\theta = 45^\circ$, $F = 4.9 \times 10^5$ V m $^{-1}$; (d) $\theta = 60^\circ$, $F = 4.9 \times 10^5$ V m $^{-1}$; (e) $\theta = 30^\circ$, $F = 2.82 \times 10^5$ V m $^{-1}$. The upper horizontal line shows scale of orbits (a)–(c) and (e). The lower line shows the scale of orbit (d), which is reduced by a factor of 2. Inset: orientation of \mathbf{B} .

to 60° , so that $\omega_B = 3\omega_c \cos\theta$ for the F and B values used in Figs. 2(d) and 2(e) (which show different PSs constructed from the *same* orbits), the chaotic sea is no longer bounded. It forms a SW whose filaments extend farther from the origin (in principle, to infinity) as time increases. Figures 2(d) and 2(e) show that part of the SW formed over 10^4 periods T_0 . Its filaments enmesh stable islands, which are remnants of the invariant curves found for smaller θ . Since an electron can diffuse *ad infinitum* along the SW filaments, it can, in principle, travel arbitrarily far along x .

The phase space of the KHO contains an infinite SW whenever the resonance condition $\omega_B = n\omega_c \cos\theta$ ($n = 1, 2, 3, \dots$) is satisfied [10]. In stroboscopic PSs, such as Figs. 2(e) and 2(f), the SW contains both ringlike and $2n$ radial filaments [10,16]. The width of the filaments $f(p_L, \theta) \approx \exp[-(p_L/\alpha \tan^3\theta)^{1/2}]$, where $\alpha \approx 1.7 \times 10^{-27} \text{ kg ms}^{-1}$ for the SL considered here [10]. In Fig. 2(e), the filaments are so thick near the web center that they overlap to form a chaotic core, similar to that in Fig. 2(c). Outside this core, f decreases so rapidly that electrons rarely diffuse farther than $\sim 10^{-25} \text{ kg ms}^{-1}$ from the origin, which corresponds to an x displacement of $\sim 100d$.

Figure 3(d) shows a finite part of the chaotic trajectory, starting from rest, which generates the SW in Figs. 2(d) and 2(e). This orbit extends approximately 4.5 times farther along x than that in Fig. 3(c), which is confined to the chaotic core of Fig. 2(c) [note that, in Fig. 3, the scale of orbit (d) is compressed by a factor of 2]. Figure 2(f) shows an $n = 1$ SW for $\theta = 30^\circ$. This angle is small enough to produce narrow web filaments (even near the origin) which confine the electrons to delocalized quasiregular orbits [Fig. 3(e)]. At each resonance, unbounded diffusion through the SW enables electrons to progress rapidly through the SL. But moving F , B , or θ off resonance destroys the SW, thereby localizing the electrons and impeding their flow. Changing these parameters should therefore modulate the electron drift velocity v_d , which is proportional to the scattering-induced current I [14].

To quantify this effect, we calculated v_d for electrons starting from rest by using the kinetic formula [17]

$$v_d = \tau^{-1} \int_0^\infty \exp(-t/\tau) v_x(t) dt, \quad (3)$$

where $v_x(t) = \hbar^{-1} \partial E(\mathbf{k}(t)) / \partial k_x$, and the scattering time $\tau = 1 \text{ ps}$ is determined from experiment [14]. We emphasize that similar results are obtained for a wide range of initial conditions.

When $\theta = 0^\circ$, Eq. (3) gives the Esaki-Tsu $v_d(F)$ relation [18], shown by the dashed curve in Fig. 4. This curve has a maximum at the field $F_B = 6.2 \times 10^4 \text{ V m}^{-1}$ for which $\omega_B \tau = 1$. When $F \lesssim F_B$, for all θ , the electrons traverse only short, almost linear, orbital segments before scattering, and so the distinction between regular and chaotic trajectories is lost. Consequently, in Fig. 4, the

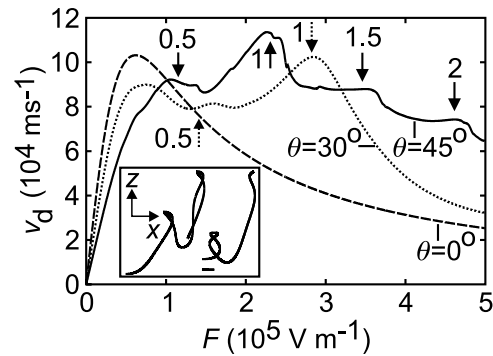


FIG. 4. Dashed (dotted) [solid] curves: $v_d(F)$ for $\theta = 0^\circ$ (30°) [45°] and $B = 2 \text{ T}$. Solid (dotted) arrows mark expected positions of resonant peaks for $\theta = 45^\circ$ (30°) with specified n and r . Inset: electron orbits in x - z plane for $0 < t < 4\tau$ and $\theta = 45^\circ$, with $F = 2.3 \times 10^5 \text{ V m}^{-1}$ (left) and $5 \times 10^5 \text{ V m}^{-1}$ (right). The horizontal line shows a peak-to-peak amplitude of Bloch oscillation at $F = 5 \times 10^5 \text{ V m}^{-1}$.

$v_d(F)$ plots are all approximately Ohmic when $F \lesssim F_B$. In this regime, v_d is lower when $\theta \neq 0^\circ$ because the in-plane (z) component of \mathbf{B} bends the electron trajectories and transfers momentum out of the x direction [17]. For $F \gtrsim 2F_B$, the $v_d(F)$ curves for $\theta = 30^\circ$, and 45° lie well above the 0° trace because the mean-free path is long enough to ensure that electrons in chaotic trajectories travel farther along x before scattering than those performing Bloch oscillations. To illustrate this, the right-hand orbit in the (boxed) inset of Fig. 4 shows an unstable trajectory for $\theta = 45^\circ$ and $F = 5 \times 10^5 \text{ V m}^{-1}$ over the time interval $0 < t < 4\tau$ which dominates the integral in Eq. (3). The x displacement of an electron in this orbit is ~ 5 times the amplitude of the corresponding 0° Bloch oscillation (horizontal line in Fig. 4 inset). This chaos-induced orbital delocalization increases v_d and the electrical conductivity.

When $\theta = 45^\circ$, $v_d(F)$ has a pronounced maximum (upward solid arrow in Fig. 4) at $F \approx 2.3 \times 10^5 \text{ V m}^{-1}$. For this F , $\omega_B = \omega_c \cos\theta$ ($n = 1$ resonance), and the phase space contains an unbounded SW similar to that in Fig. 2(f). The electron undergoes rapid diffusive motion through the SW (left-hand orbit in Fig. 4 inset), and so travels farther along x before scattering than when F is off resonance. The $n = 2$ resonance at $\theta = 45^\circ$ also produces a clear peak in $v_d(F)$ (right-hand arrow in Fig. 4). When $\theta = 30^\circ$, $v_d(F)$ contains a large $n = 1$ maximum (downward dotted arrow in Fig. 4) originating from the unbounded quasiregular trajectory in Fig. 3(e).

When $\omega_B = r\omega_c \cos\theta$ where r is a noninteger rational number, the PSs contain a *finite* SW which, though enclosed by stable islands [11], delocalizes the electrons sufficiently to generate peaks in $v_d(F)$. In Fig. 4, the 45° $v_d(F)$ curve reveals $r = 0.5$ and 1.5 resonant peaks, plus weaker features associated with other r values. The 30° trace has a small maximum near the $r = 0.5$ resonance.

Figure 5 shows color contour plots of $v_d(F, \theta)$ for a range of B . A small field of 0.5 T [Fig. 5(a)] is insufficient

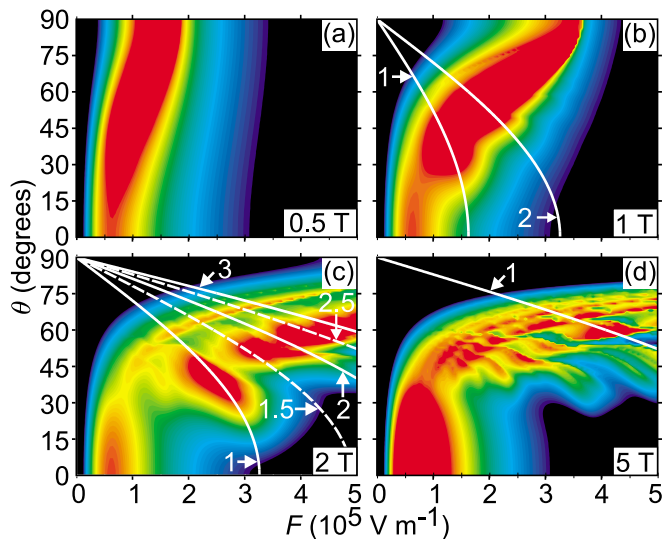


FIG. 5 (color). $v_d(F, \theta)$ [black (low) and red (high)] for $B =$ (a) 0.5 T, (b) 1 T, (c) 2 T, and (d) 5 T. Solid (dashed) white curves show loci of numbered n (r) resonances.

to drive the electron motion chaotic. As θ increases, the in-plane component of \mathbf{B} transfers more momentum out of the x direction, and thus the F value required for peak v_d increases [17]. When $B = 1$ T [Fig. 5(b)], chaotic diffusion through SWs begins to affect the SL conductivity. The red area of maximal v_d is weakly modulated by $n = 1$ and 2 resonances whose (F, θ) loci are shown by the left-hand and right-hand white curves respectively. The SW-induced resonant peaks become stronger as B , and the driving term in Eq. (2), increases. At $B = 2$ T [Fig. 5(c)], distinct islands of v_d maxima originate from several n (r) resonances whose loci are shown by solid (dashed) white curves. The $n = 1$ (left-hand) island is most pronounced for $20^\circ \lesssim \theta \lesssim 50^\circ$. For $\theta \lesssim 20^\circ$, the driving term in Eq. (2) is too small to produce rapid SW diffusion. By contrast, for $\theta \gtrsim 50^\circ$, it is large enough to ensure that the chaotic paths are extended for all $F \lesssim 2 \times 10^5$ V m $^{-1}$. Further elongation along x of the orbit at the $n = 1$ resonance therefore has a negligible effect on v_d . A field of 5 T [Fig. 5(d)] produces a complex pattern of peaks originating mainly from $r < 1$ resonances.

Since the resonance condition is independent of electron energy, the peaks in $I(V)$ should be observable when, in a real device, electrons are injected with a range of energies. It is also necessary that broadening mechanisms do not disrupt MB conduction. This requires liquid helium temperatures so that $\tau \gtrsim 1$ ps [14] and $\omega_B \tau > 1$ for electric fields low enough to preserve the MB and give negligible Zener tunneling. The latter condition is easily met by tailoring the SL composition to provide a large MB gap. Broadening due to monolayer growth fluctuations can routinely be made $\ll \Delta$. For $B = 0$ T, $I(V)$ data are in excellent quantitative agreement with the Esaki-Tsu curve [14]. Since our calculations for chaotic electron dynamics are based

on the same semiclassical model, the resonances predicted by our calculations should also be observable for both two- and three-terminal SLs.

In summary, we have shown that the unique phase space structure of non-KAM systems can have a pronounced effect on the conductivity of condensed matter. Despite involving only *time-independent* fields, the SL system corresponds to a 1D KHO, whose orbits are extended by the onset of chaos and produce resonant maxima in $v_d(F)$. For certain B values, quantum suppression of SW diffusion [15] is expected, and so SLs might provide an experimentally accessible environment for studying quantum chaos and localization in non-KAM systems. Similar dynamics might be realized in other periodic systems, including optical lattices [19].

This work was supported by The Royal Society, The British Council, EPSRC UK, CONACyT (Mexico), and KBN (Poland) Grant No. PB 2 P03B 05518.

*On leave from Universidad Autonoma de Puebla, Mexico.

†Present address: Institute of Physics, Wroclaw University of Technology, Poland.

- [1] For a review, see *Quantum Chaos—An Introduction*, edited by H.-J. Stöckmann (Cambridge University Press, Cambridge, 1999).
- [2] F. L. Moore *et al.*, Phys. Rev. Lett. **73**, 2974 (1994).
- [3] C. M. Marcus *et al.*, Phys. Rev. Lett. **69**, 506 (1992).
- [4] A. M. Chang *et al.*, Phys. Rev. Lett. **73**, 2111 (1994).
- [5] J. P. Bird *et al.*, Phys. Rev. Lett. **82**, 4691 (1999).
- [6] D. Weiss *et al.*, Phys. Rev. Lett. **70**, 4118 (1993).
- [7] T. M. Fromhold *et al.*, Phys. Rev. Lett. **72**, 2608 (1994); **75**, 1142 (1995).
- [8] K. J. Luo *et al.*, Phys. Rev. Lett. **81**, 1290 (1998); J. Kastrup *et al.*, Appl. Phys. Lett. **65**, 1808 (1994).
- [9] K. N. Alekseev *et al.*, Phys. Rev. B **54**, 10625 (1996).
- [10] *Weak Chaos and Quasi-Regular Patterns*, edited by G. M. Zaslavsky *et al.* (Cambridge University Press, Cambridge, 1991); D. I. Kamenev and G. P. Berman, *Quantum Chaos: A Harmonic Oscillator in a Monochromatic Wave* (Rinton Press, Princeton, NJ, 2000).
- [11] P.-K. Chia, L. Schmitz, and R. W. Conn, Phys. Plasmas **3**, 1545 (1996).
- [12] S. A. Gardiner, J. I. Cirac, and P. Zoller, Phys. Rev. Lett. **79**, 4790 (1997).
- [13] B. Hu *et al.*, Phys. Rev. Lett. **82**, 4224 (1999).
- [14] C. Rauch *et al.*, Phys. Rev. Lett. **81**, 3495 (1998).
- [15] V. Ya. Demikhovskii, D. I. Kamenev, and G. A. Luna-Acosta, Phys. Rev. E **52**, 3351 (1995); **59**, 294 (1999).
- [16] For non-cosinusoidal $E(k_x)$, the SHO is driven by a harmonic series of plane waves, which produces more complex SW patterns [10].
- [17] H. J. Hutchinson *et al.*, J. Appl. Phys. **75**, 320 (1994).
- [18] L. Esaki and R. Tsu, IBM J. Res. Dev. **14**, 61 (1970).
- [19] T. M. Fromhold *et al.*, J. Opt. B: Quantum Semiclass. Opt. **2**, 628 (2000).